



Short communication

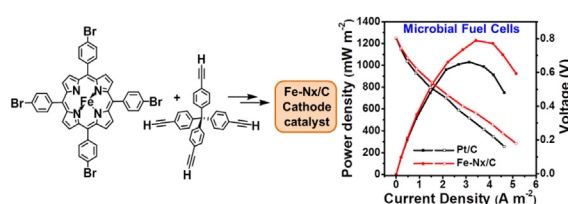
Iron-rich nanoparticle encapsulated, nitrogen doped porous carbon materials as efficient cathode electrocatalyst for microbial fuel cells

Guolong Lu^{a,b}, Youlong Zhu^b, Lu Lu^c, Kongliang Xu^a, Heming Wang^c, Yinghua Jin^b, Zhiyong Jason Ren^c, Zhenning Liu^{a,*}, Wei Zhang^{b,*}^a Key Laboratory of Bionic Engineering (Ministry of Education), Jilin University, Changchun, Jilin Province, 130022, PR China^b Department of Chemistry and Biochemistry, University of Colorado, Boulder, CO 80309, USA^c Department of Civil, Environmental and Architectural Engineering, University of Colorado, Boulder, CO 80309, USA

HIGHLIGHTS

- A porous N-doped carbon material (Fe-N_x/C) was prepared from simple building blocks.
- Catalytic performance of Fe-N_x/C was investigated for oxygen reduction reaction.
- Fe-N_x/C was applied in microbial fuel cell as an efficient cathode catalyst.

GRAPHICAL ABSTRACT



ARTICLE INFO

Article history:

Received 4 December 2015

Received in revised form

19 February 2016

Accepted 8 March 2016

Keywords:

Electrocatalyst

Oxygen reduction reaction

Microbial fuel cell

Nitrogen-doped carbon

Porous organic polymer

ABSTRACT

Developing efficient, readily available, and sustainable electrocatalysts for oxygen reduction reaction (ORR) in neutral medium is of great importance to practical applications of microbial fuel cells (MFCs). Herein, a porous nitrogen-doped carbon material with encapsulated Fe-based nanoparticles (Fe-N_x/C) has been developed and utilized as an efficient ORR catalyst in MFCs. The material was obtained through pyrolysis of a highly porous organic polymer containing iron(II) porphyrins. The characterizations of morphology, crystalline structure and elemental composition reveal that Fe-N_x/C consists of well-dispersed Fe-based nanoparticles coated by N-doped graphitic carbon layer. ORR catalytic performance of Fe-N_x/C has been evaluated through cyclic voltammetry and rotating ring-disk electrode measurements, and its application as a cathode electrocatalyst in an air-cathode single-chamber MFC has been investigated. Fe-N_x/C exhibits comparable or better performance in MFCs than 20% Pt/C, displaying higher cell voltage (601 mV vs. 591 mV), maximum power density (1227 mW m⁻² vs. 1031 mW m⁻²) and Coulombic efficiency (50% vs. 31%). These findings indicate that Fe-N_x/C is more tolerant and durable than Pt/C in a system with bacteria metabolism and thus holds great potential for practical MFC applications.

© 2016 Elsevier B.V. All rights reserved.

1. Introduction

Microbial fuel cell (MFC) is a bio-electrochemical technology that converts chemical energy in organic compounds to electricity

by the metabolism of anaerobic bacteria [1]. The bacteria decompose organic fuel in the anode compartment, generating CO₂, electrons, and protons. Electrons and protons migrate to the cathode to unite with an oxidizing agent, which is oxygen in most cases [2]. Unfortunately, the sluggish kinetics of oxygen reduction reaction (ORR) has become the bottleneck of power generation in MFCs, which function in pH-neutral aqueous electrolyte with lower concentration of H⁺ or OH⁻, unlike acidic or alkaline electrolyte in fuel

* Corresponding authors.

E-mail addresses: liu_zhenning@jlu.edu.cn (Z. Liu), Wei.Zhang@colorado.edu (W. Zhang).

cells. Platinum-based catalyst has been considered as the most commonly used ORR catalyst for fuel cells. However, the high cost, scarcity, and limited stability of such precious-metal catalyst have hindered their applications. In addition, it has been reported that Pt/C system is very sensitive to pollutants present naturally in wastewater and easily poisoned [3].

It has attracted broad interest to develop sustainable, efficient, and durable electrocatalysts for ORR. To date, a variety of ORR electrocatalysts have been developed, such as metal-free carbon materials [4–6] and non-precious metal based catalysts [7–14], which are aimed at affordable alternatives in place of Pt-based catalysts. Composites of metal and nitrogen-doped carbon (M-N_x/C) are a class of non-precious metal ORR catalysts that are often produced by pyrolysis of metallo-porphyrin or -phthalocyanine precursors. Jasinski and coworker first showed ORR activities of Fe-N_x/C derived from iron(II)-phthalocyanines in fuel cells [15]. Subsequently, various Fe-N_x/C catalysts have been reported to exhibit comparable or even higher ORR activity than commercial Pt/C system, when they are applied in fuel cells with acidic or alkaline electrolyte [16–19]. The first example of a MFC cathode catalyst based on M-N_x/C (M = Fe or Co) was reported by Schröder and coworkers, which show a good activity in neutral electrolyte [11]. Since then, development of readily available and sustainable M-N_x/C catalysts that exhibit good performance in MFC has been an active research area with the goal of replacing currently used expensive and scarce Pt/C system [20–24]. Recently, nitrogen-doped carbon materials derived from pyrolysis of porous polymers have attracted great attention. It has been reported that high porosity can facilitate mass transport, thus is important for M-N_x/C to function as an efficient ORR catalyst [25]. Given a plethora of organic porous materials with various compositions, we envision that efficient ORR catalyst could be obtained through judicious selection of building blocks. In this work, iron-rich nanoparticle encapsulated, nitrogen doped porous carbon material (Fe-N_x/C) has been developed as efficient non-precious metal ORR catalyst, through pyrolysis of a porous organic polymer containing iron(II) metallated porphyrins (FePOP). The successful application of such materials as the cathode electrocatalyst in a single-chamber MFC was also demonstrated.

2. Experimental

2.1. Preparation and pyrolysis of FePOP

To a 100 mL Schlenk tube were added iron (II)-5,10,15,20-tetrakis-(4'-bromophenyl)porphyrin (M1) (100 mg, 0.10 mmol), tetrakis(4-ethynylphenyl)methane (M2) (42 mg, 0.10 mmol), Pd(PPh₃)₂Cl₂ (26 mg, 0.036 mmol) and CuI (4.0 mg, 0.021 mmol), followed by triethylamine (5 mL) and anhydrous DMF (15 mL) as the solvent (Scheme S1). The resulting solution was degassed through three evacuation-nitrogen refill cycles and heated at 100 °C for 2 days under nitrogen atmosphere. It was then cooled to room temperature, and water (10 mL) was added. The mixture was sonicated for 10 min and the solid was filtered. The solid was successively washed with water (2 × 30 mL), ethanol (2 × 30 mL), dichloromethane (2 × 30 mL) and acetone (2 × 30 mL), and dried in vacuo to give the product (FePOP) as a dark solid (100 mg, 91%). Elemental analysis for FePOP: Calculated for (C₇₇H₄₀N₄Fe)_n: C, 85.87%; H, 3.74%; N, 5.20%; Fe, 5.19%; Found: C, 70.43%; H, 3.49%; N 3.91%; Fe, 3.38%. FePOP (50 mg) was pyrolyzed in a furnace under Ar atmosphere at 800 °C [18,26,27], to obtain the pyrolyzed materials (FePOP-800, 43 mg, 86% weight recovery). Then FePOP-800 (40 mg) was ultrasonically leached in 6 M HCl for 6 h to remove Fe element that was not well encapsulated in carbon materials during pyrolysis. Fe-N_x/C (37 mg) was obtained after filtration and vacuum drying. Based on the raw materials, the cost of Fe-N_x/C was

estimated to be ~8.6 USD g⁻¹, substantially lower than that of Pt/C (150 USD g⁻¹) [29].

2.2. Material characterization

To characterize the structure of the obtained electrocatalyst, transmission electronic microscopy (TEM) images were obtained with a F-30ST transmission electron microscope (Tecnai, US) on Cu substrate. Powder X-ray diffraction (PXRD) data was obtained with an X-ray diffractometer (Bruke D8 Adv., Germany) equipped with Cu K α source at step scan of 0.02° over the range of 10°–90°. The resulting PXRD data were analyzed with the Powder Diffraction Standard (JCPDS) database. The elemental composition of samples were examined and analyzed by energy dispersive X-ray spectroscopy (EDS) and X-ray photoelectron spectroscopy (XPS, Kratos-Axis UL TRA DLD). The Quantachrome Autosorb ASiQ automated gas sorption analyzer was used to measure N₂ adsorption isotherms. The samples were activated by heating at 120 °C under vacuum for at least 22 h prior to the analysis. Ultrahigh purity grade (99.999% purity) N₂ and He, oil-free valves and gas regulators were used for all free space corrections and measurements.

2.3. MFC setup and electrode preparation

Single-chamber MFCs were used in the experiments. The anode was a carbon fiber brush (4 cm in diameter, 2 cm in the length). The cathode was an air-cathode fabricated as described in the literature [28]. The anode and cathode were installed in a plexiglass tube chamber with a length of 4 cm, a diameter of 3 cm and a total volume of 19.8 mL [29,30]. The test cathode of Fe-N_x/C was prepared by pasting the sonicated mixture of Fe-N_x/C and carbon black (Vulcan XC-72) in the weight ratio of 1:1 with the assistance of 5% Nafion. The control electrode of Pt/C (20 wt%) was prepared as described by other groups [23,31]. Fe-N_x/C (2 mg cm⁻²) and Pt (0.5 mg cm⁻²) were used in the electrochemical measurements and MFC experiments, respectively.

All MFCs were inoculated with an effluent obtained from the same MFC reactor, which has been operating for several years in the lab, in order to warrant similar microbial functions. After the inoculation, the MFC was fed with phosphate buffer saline (PBS, 0.1 M, pH = 7.0) containing NaAc (1.0 g L⁻¹), KCl (0.13 g L⁻¹), and NH₄Cl (0.31 g L⁻¹), and also supplemented with mineral solution (12.5 mL L⁻¹) and vitamin solution (5 mL L⁻¹) [32]. All tests were carried out at room temperature (around 25 °C). We evaluated the performance of Fe-N_x/C and Pt/C in two parallel MFC reactors with the same inoculum and anodes but different cathodes (Pt/C cathode or Fe-N_x/C cathode). The reproducibility of the power output was tested by switching Pt/C cathode and Fe-N_x/C cathode between the two parallel MFC reactors multiple times. The variation of cell voltages with such a change was all within the experimental error each time, showing almost constant cell voltage for the MFC with Fe-N_x/C cathode, and also the one with Pt/C cathode. For each trial, the cell voltage of MFC with Fe-N_x/C cathode was consistently higher than that of the MFC with Pt/C cathode, while the anodes' potentials were almost same for the two MFCs, suggesting the repeatability and reliability of our study. We refilled the nutrient solution every ~50 h, when the voltage dropped below ~100 mV in each reactor.

2.4. Electrochemical measurement and calculation

Electrochemical measurements of cyclic voltammetry (CV) were performed using a computer-controlled potentiostat (CHI 850D, Shanghai CH Instrument, China). Rotating ring-disk electrode (RRDE) experiments were performed using a computer-controlled

potentiostat (Pine Instrument Company, USA) with a three-electrode cell system. A ring-disk (Pt-glass carbon) electrode (Autolab), a Ag/AgCl (KCl saturated) electrode (Pine, F0DR-0021), and a Pt wire were used as the working electrode, the reference electrode, and the counter electrode, respectively. The electrochemical experiments were conducted in O₂-saturated aqueous 0.1 M PBS electrolyte for the oxygen reduction reaction. The potential range was cyclically scanned between 0.4 V and −0.6 V in aqueous 0.1 M PBS at a scan rate of 10 mV s^{−1} at room temperature after purging with O₂ or Ar for 25 min. RRDE measurements were carried out at 2500 rpm [33]. The electron transfer numbers (*n*) were calculated from RRDE measurements based on the disk current (*I*_{disk}) and ring current (*I*_{ring}) using the equation (1):

$$n = 4I_{\text{disk}} / (I_{\text{disk}} + I_{\text{ring}}/N) \quad (1)$$

The percentages of hydrogen peroxide (H₂O₂) were determined by the equation (2):

$$\%H_2O_2 = \frac{200I_{\text{ring}}/N}{I_{\text{disk}} + I_{\text{ring}}/N} \quad (2)$$

where *N* is the current collection efficiency of the Pt ring and equals to 25.6%.

The Coulombic efficiency over time was calculated using the equation (3):

$$\varepsilon_{\text{Cb}} = \frac{8 \int_0^{\Delta t} I dt}{F v_{\text{An}} \Delta \text{COD}} \quad (3)$$

where *v*_{An} is the volume of liquid in the anode chamber and ΔCOD is the change of COD over time *t*.

The cell voltage (*V*_{cell}, V) across stepwise external resistances (*R*_{EX}, 5000–50 Ω) was collected every 10 min by using a data acquisition multimeter (Keithley, U.S.). The power density (*P*, mW m^{−2}) was calculated by *P* = *V*_{cell}²/(*A*·*R*_{EX}), in which *A* (7 cm²) is the geometric area of the cathode. The electrode potential was individually measured against Ag/AgCl reference.

3. Results and discussion

Fe-porphyrins and tetrapropyl connectors in a pyramidal geometry were selected as the building blocks to prepare 3D porous organic polymer. The polymer FePOP was obtained in a straightforward manner through one step Sonogashira cross-coupling reaction. FePOP was then heated at 800 °C to yield the pyrolyzed material (FePOP-800), which was ultrasonically leached in 6 M hydrochloric acid (HCl) at 90 °C for 6 h to remove iron nuclei not encapsulated by carbon materials to obtain Fe-N_x/C. As aforementioned, porosity is an important characteristic for catalysts to ensure efficient mass transport during ORR catalysis. Thus, the porous nature of the materials was evaluated by N₂ adsorption isotherm measurement with freshly activated samples (Fig. 1b). The Brunauer-Emmett-Teller (BET) surface area (*S*_{BET}) of FePOP is calculated to be 854 m² g^{−1}, which is much higher than those of small molecule-based cathode catalysts [34,35]. It was observed that the pyrolysis of FePOP and subsequent leaching with HCl decrease the porosity of the material, which is likely due to the collapse of the 3D polymer network structure during carbonization and leaching. Nevertheless, the pyrolyzed FePOP-800 and leached Fe-N_x/C still show *S*_{BET} of 608 m² g^{−1} and 343 m² g^{−1} respectively. HR-TEM imaging reveals the presence of abundant well-dispersed nanoparticles in Fe-N_x/C (Fig. 1c). The examination of elemental mapping shows that these nanoparticles mainly consist of Fe

element (Figure S2). The *d*-spacing of these Fe-based nanoparticles is approximately 0.239 nm (Fig. 1d), which is much larger than the standard value for Fe (0.203 nm, JCPDS 06-0696) but is in line with the value of Fe₂N lattice (0.24 nm, JCPDS 54-58735). The lattice *d*-spacing of the outer surface of these nanoparticles is found to be 0.34 nm (Fig. 1d), which is in good agreement with that of graphitic carbon [27,36]. These results indicate that these Fe-based nanoparticles have survived leaching likely under the protection of the graphitic carbon layer. These findings have been corroborated by the XRD profile of Fe-N_x/C, which displays peaks at 2θ ≈ 23°, 41° and 43° (Figure S3), corresponding to (002) plane of graphitic carbon [23], and (200) and (121) planes of Fe₂N, respectively [37].

The chemical composition of Fe-N_x/C catalyst was further examined by energy dispersive X-ray spectroscopy (EDS) and X-ray photoelectron spectroscopy (XPS) (Figure S4 and Figure S5). EDS shows that Fe-N_x/C contains C (ca. 56.49 wt%), Fe (ca. 3.17 wt%), O (ca. 7.80 wt%), N (ca. 2.77 wt%) and Cu (ca. 29.76 wt%) as well as a small amount of Pd, Si and Cl. The Pd element is likely introduced during the Sonogashira coupling step, Si and Cl elements are likely from the pyrolysis and leaching steps, and the presence of Cu could be explained by the substrate used in the test. The XPS spectrum exhibits peaks that correspond to C_{1s} (ca. 83.08 wt%), N_{1s} (ca. 0.86 wt%), O_{1s} (ca. 15.08 wt%), Fe_{2p} (ca. 0.13 wt%), and Cl_{2p} (ca. 0.85 wt%). It is noteworthy that the surface contents of Fe and N from XPS measurements are much lower than those estimated from EDS measurements, suggesting that the majority of Fe and N elements are located in the nanoparticles encapsulated by graphitic carbon. This is also consistent with the observation from HR-TEM that the Fe-based nanoparticles are surrounded by graphitic layer. The curve of C_{1s} can be fitted by C-C, C=N, C-N and O-C=O peaks (Figure S5b) [38], and the N_{1s} profile can be reclassified into four components: pyridinic N (398.5 eV), Fe-N (399.5 eV), pyrrolic N (400.6 eV) and graphitic N (401.1 eV) [16,17,25]. These data indicate that the graphitic carbon layer contains N elements in various forms, which is of great significance for ORR catalysis. It has been demonstrated that graphitic N could improve the limiting-diffusion-current, whereas pyridinic N could raise the onset potential and even change the ORR mechanistic pathway from a 2-electron-dominated process to a 4-electron-dominated process [39,40]. The XPS survey of Fe_{2p} shows a high signal-noise ratio of 1:1 (Figure S5d) [23,37], implying that Fe atoms are covered and not readily detectable by XPS, in line with HR-TEM observations.

We then investigated the electrocatalytic activity of Fe-N_x/C by cyclic voltammetry (CV) in Ar- and O₂-saturated 0.1 M PBS (pH = 7) at 10 mV s^{−1}. As shown in Fig. 2a, Fe-N_x/C exhibits an obvious cathodic peak (0.05 V vs. Ag/AgCl) in O₂-saturated 0.1 M PBS, which is absent in Ar-saturated solution, indicating the peak observed in O₂-saturated neutral medium is indeed from electrocatalysis of ORR. For comparison purpose, we also examined the electrocatalytic activity of commercial Pt/C (20 wt%) under the same conditions. Pt/C system shows more positive cathodic peak (0.11 V vs. Ag/AgCl), whereas Fe-N_x/C displays larger ORR peak current and capacitance current.

Two possible ORR pathways exist: one is direct 4-electron pathway, where O₂ is reduced to water in one step; the other one is indirect 2-electron pathway, where hydrogen peroxide (H₂O₂) is produced as an intermediate. The generation of H₂O₂ will not only lower the output voltage of MFCs, but also reduce energy conversion efficiency, corroding electrocatalyst on the cathode and impairing microbial layer on the anode of single-chamber MFCs. Hence, we investigated the catalytic mechanism and H₂O₂ production of Fe-N_x/C-catalyzed ORR by rotating ring-disk electrode (RRDE) measurement. As shown in Fig. 2b, the current responses of RRDE measurement for Fe-N_x/C are comparable to those of benchmark Pt/C, displaying large disk currents with relatively low ring currents. The onset potential of Fe-N_x/C cathode in neutral

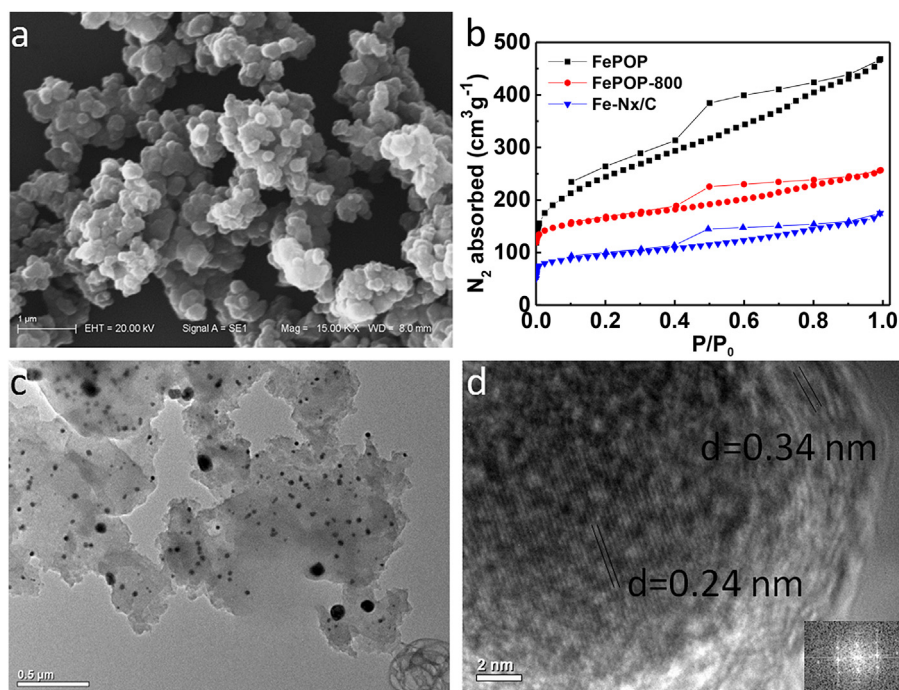


Fig. 1. SEM image of FePOP (a), Nitrogen adsorption isotherms (77 K) of FePOP, FePOP-800, and Fe-N_x/C (b); HR-TEM images Fe-N_x/C (c and d). All samples were prepared by drop-casting the suspension of the material in ethanol.

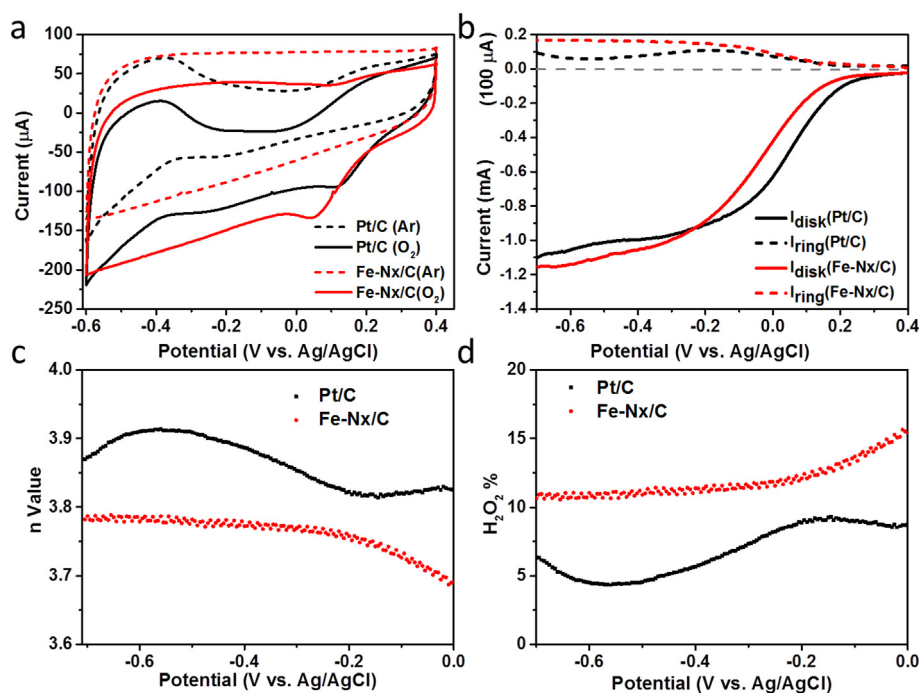


Fig. 2. Cyclic voltammetry (CV) curves of Fe-N_x/C and Pt/C in O₂- and Ar-saturated 0.1 M PBS (a); Rotating Ring-Disk Electrode (RRDE) curves of Fe-N_x/C and Pt/C in O₂-saturated 0.1 M PBS at 2500 rpm (b), and corresponding electron transfer number n (c), and H₂O₂ yield (d). The scan rate was 10 mV s⁻¹ for CV and RRDE measurements.

medium (0.1 M PBS) was 0.19 V, comparable to that of Pt/C system (0.20 V). The production of H₂O₂ on Fe-N_x/C and Pt/C catalysts was respectively 10–15% and 6–8% in the plateau region (0.0 V to -0.7 V). The number of electrons transferred under the catalysis of Fe-N_x/C was calculated to be 3.77 ± 0.4 , which is close to 4 and comparable to the result obtained for the Pt/C catalyst ($n = 3.88 \pm 0.4$). (Fig. 2c). Our study suggests that, although 2-

electron path is present, 4-electron pathway is dominant in the ORR catalyzed by Fe-N_x/C. The diffusion current density of Fe-N_x/C (6.0 mA cm^{-2} , 1.2 mA) is comparable to Pt/C (5.8 mA cm^{-2} , 1.1 mA).

The performance of the Fe-N_x/C electrocatalyst was further evaluated in an air-cathode single-chamber MFC and compared to the reactors with Pt/C cathodes in terms of cell voltage and power density. The MFCs were operated for about 14 cycles in 900 h with

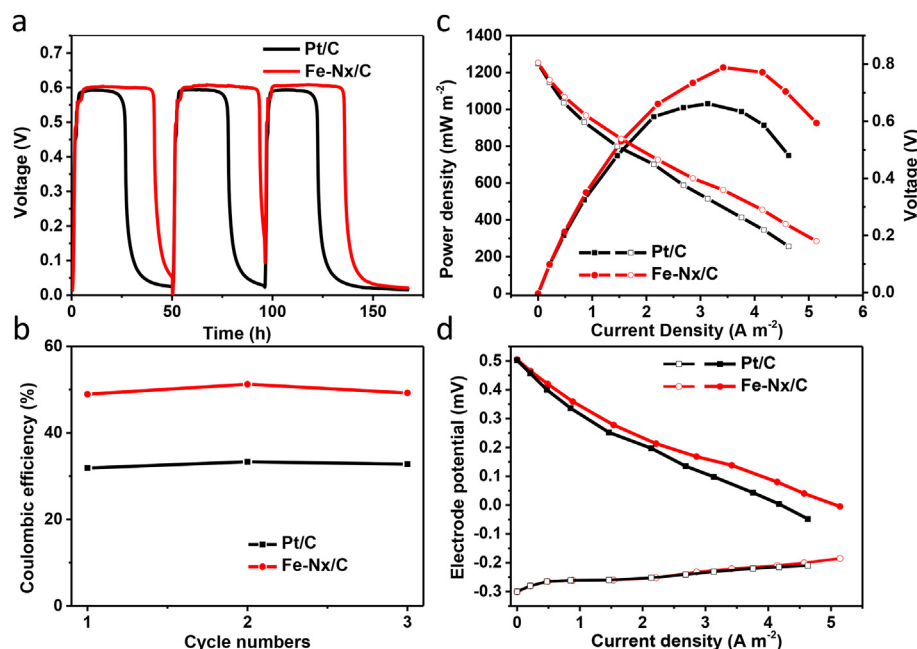


Fig. 3. The cell cycle voltage (a), Coulombic efficiency corresponding to the cycles in Fig. 3a (b), power density curves (filled symbols) and polarization curves (hollow symbols) (c), and electrode potentials (filled symbols for cathode and hollow symbols for anodes) (d) of MFCs when Pt/C or Fe-N_x/C were used as the cathode electrocatalyst. The cell voltages of MFCs run for 14 cycles in 900 h are shown in Fig. S6.

stable performance (Figure S6), and the data of 3 cycles during the last 150 h are shown in Fig. 3. Although in pH-neutral medium, Fe-N_x/C does not show significant advantages in ORR catalytic performance, we found Fe-N_x/C performs better than the commercial 20 wt% Pt/C under the conditions of MFC. As shown in Fig. 3a, MFC using Fe-N_x/C as the electrocatalyst displays a stable output voltage of 602 mV, whereas it was 591 mV for Pt/C-based MFC. We observed much enhanced (56% increase) Coulombic efficiency for MFC using Fe-N_x/C as the catalyst, compared to the case of Pt/C based MFC (~50% vs. ~32%) (Fig. 3b). The Coulombic efficiency of MFCs with Pt/C cathode obtained in our study is consistent with the literature report by Logan [10].

Finally, we examined power density and corresponding electrode potentials for MFC using Pt/C or Fe-N_x/C cathodes. Consistent with the previous findings, MFC with Fe-N_x/C showed higher cell voltage (Fig. 3c) and cathode potential (Fig. 3d) than those of Pt/C-based MFC. More importantly, the maximum power density for Fe-N_x/C reaches 1227 mW m⁻² at 3.41 A m⁻², which is 19% higher than that observed for Pt/C (1031.4 mW m⁻² at 3.13 A m⁻²). Since the anodic potentials of Pt/C based MFC and Fe-N_x/C based MFC are similar (Fig. 3d), the improved power generation of the latter is mainly conferred by the cathode containing Fe-N_x/C catalyst. The enhanced performance of Fe-N_x/C based MFC is probably due to the enhanced stability of such nitrogen-doped porous carbon catalyst in the MFC medium with abundant metabolized products of bacteria, compared to Pt/C system.

4. Conclusion

Fe-N_x/C composites have been obtained from a highly porous and readily available metallo-porphyrin polymer and applied as a cathodic catalyst in single-chamber MFC. Fe-N_x/C displays excellent ORR activity in pH-neutral medium, which is likely due to a synergistic process by Fe-based nanoparticles and N-doped graphitic carbon layer. Moreover, MFC using Fe-N_x/C catalyst demonstrates higher performance than that using Pt/C, in terms of cell voltage,

maximum power density and Coulombic efficiency. Our study indicates Fe-N_x/C is more tolerant and durable than Pt/C in a MFC system with bacteria metabolism, suggesting the potential application of such a non-precious metal based, readily accessible catalyst as an alternative to the current Pt/C system.

Acknowledgement

This work was supported by National Science Foundation (DMR-1055705), National Natural Science Foundation of China (51375204), Jilin Provincial Science & Technology Department (20130727033YY and 20140101056JC) and Project “985” on Engineering Bionics of Jilin University. The authors thank Prof. Xiaobo Yin and Dr. Yao Zhai for the help with pyrolysis experiments.

Appendix A. Supplementary data

Supplementary data related to this article can be found at <http://dx.doi.org/10.1016/j.jpowsour.2016.03.028>.

References

- [1] B.E. Logan, *Microbial Fuel Cells*, John Wiley & Sons, Inc., 2008.
- [2] H.M. Wang, Z.Y.J. Ren, *Biotechnol. Adv.* 31 (2013) 1796–1807.
- [3] C. Santoro, A. Serov, C.W.N. Villarrubia, S. Stariha, S. Babanova, K. Artyushkova, A.J. Schuler, P. Atanassov, *Sci. Rep. U. K.* 5 (2015).
- [4] H. Dong, H.B. Yu, X. Wang, Q.X. Zhou, J.L. Feng, *Water Res.* 46 (2012) 5777–5787.
- [5] Y. Liu, H. Liu, C. Wang, S.X. Hou, N. Yang, *Environ. Sci. Technol.* 47 (2013) 13889–13895.
- [6] B. Zhang, Z. Wen, S. Ci, S. Mao, J. Chen, Z. He, *ACS Appl. Mater. Interfaces* 6 (2014) 7464–7470.
- [7] H.M. Wang, Z.C. Wu, A. Plaseied, P. Jenkins, L. Simpson, C. Engtrakul, Z.Y. Ren, *J. Power Sources* 196 (2011) 7465–7469.
- [8] X. Li, B.X. Hu, S. Suib, Y. Lei, B.K. Li, *J. Power Sources* 195 (2010) 2586–2591.
- [9] M. Ma, S.J. You, X.B. Gong, Y. Dai, J.L. Zou, H.G. Fu, *J. Power Sources* 283 (2015) 74–83.
- [10] S. Cheng, H. Liu, B.E. Logan, *Environ. Sci. Technol.* 40 (2006) 364–369.
- [11] F. Zhao, F. Harnisch, U. Schroder, F. Scholz, P. Bogdanoff, I. Herrmann, *Electrochem. Commun.* 7 (2005) 1405–1410.
- [12] C.H. Wang, C.T. Wang, H.C. Huang, S.T. Chang, F.Y. Liao, *RSC Adv.* 3 (2013)

- 15375–15381.
- [13] G. Lu, Y. Zhu, K. Xu, Y. Jin, Z.J. Ren, Z. Liu, W. Zhang, *Nanoscale* 7 (2015) 18271–18277.
- [14] G.L. Lu, H.S. Yang, Y.L. Zhu, T. Huggins, Z.J. Ren, Z.N. Liu, W. Zhang, *J. Mater. Chem. A* 3 (2015) 4954–4959.
- [15] R. Jasinski, *Nature* 201 (1964) 1212–1213.
- [16] K. Artyushkova, A. Serov, S. Rojas-Carbonell, P. Atanassov, *J. Phys. Chem. C* 119 (2015) 25917–25928.
- [17] S. Kabir, K. Artyushkova, B. Kiefer, P. Atanassov, *Phys. Chem. Chem. Phys.* 17 (2015) 17785–17789.
- [18] L. Lin, Q. Zhu, A.W. Xu, *J. Am. Chem. Soc.* 136 (2014) 11027–11033.
- [19] Q.P. Lin, X.H. Bu, A.G. Kong, C.Y. Mao, F. Bu, P.Y. Feng, *Adv. Mater.* 27 (2015) 3431–3436.
- [20] L. Birry, P. Mehta, F. Jaouen, J.P. Dodelet, S.R. Guiot, B. Tartakovsky, *Electrochim. Acta* 56 (2011) 1505–1511.
- [21] S.Z. Li, Y.Y. Hu, Q. Xu, J. Sun, B. Hou, Y.P. Zhang, *J. Power Sources* 213 (2012) 265–269.
- [22] B. Lai, P. Wang, H.R. Li, Z.W. Du, L.J. Wang, S.C. Bi, *Bioresour. Technol.* 131 (2013) 321–324.
- [23] Y.H. Su, H.L. Jiang, Y.H. Zhu, W.J. Zou, X.L. Yang, J.D. Chen, C.Z. Li, *J. Power Sources* 265 (2014) 246–253.
- [24] X. Ge, A. Sumboja, D. Wu, T. An, B. Li, F.W.T. Goh, T.S.A. Hor, Y. Zong, Z. Liu, *ACS Catal.* 5 (2015) 4643–4667.
- [25] S.J. You, X.B. Gong, W. Wang, D.P. Qi, X.H. Wang, X.D. Chen, N.Q. Ren, *Adv. Energy Mater.* 6 (2016).
- [26] Y. Hu, J.O. Jensen, W. Zhang, L.N. Cleemann, W. Xing, N.J. Bjerrum, Q.F. Li, *Angew. Chem. Int. Ed.* 53 (2014) 3675–3679.
- [27] Z.S. Wu, L. Chen, J.Z. Liu, K. Parvez, H.W. Liang, J. Shu, H. Sachdev, R. Graf, X.L. Feng, K. Mullen, *Adv. Mater.* 26 (2014) 1450–1455.
- [28] S. Cheng, H. Liu, B.E. Logan, *Electrochem. Commun.* 8 (2006) 489–494.
- [29] T. Huggins, H.M. Wang, J. Kearns, P. Jenkins, Z.J. Ren, *Bioresour. Technol.* 157 (2014) 114–119.
- [30] H. Wang, D. Heil, Z.J. Ren, P. Xu, *Chemosphere* 125 (2015) 94–101.
- [31] Y. Liu, H. Liu, C. Wang, S.X. Hou, N.A. Yang, *Environ. Sci. Technol.* 47 (2013) 13889–13895.
- [32] A. Haeger, C. Forrestal, P. Xu, Z.J. Ren, *Bioresour. Technol.* 174 (2014) 287–293.
- [33] H. Yazdi, L. Alzate-Gaviria, Z.J. Ren, *Bioresour. Technol.* 180 (2015) 258–263.
- [34] X. Zhang, D. Pant, F. Zhang, J. Liu, W. He, B.E. Logan, *ChemElectroChem* 1 (2014) 1859–1866.
- [35] T.M. Huggins, J.J. Pietron, H.M. Wang, Z.J. Ren, J.C. Biffinger, *Bioresour. Technol.* 195 (2015) 147–153.
- [36] C. Han, X.J. Bo, Y.F. Zhang, M. Li, A. Nsabimana, L.P. Guo, *Nanoscale* 7 (2015) 5607–5611.
- [37] Y. Liu, X.J. Jin, D.D. Dionysiou, H. Liu, Y.M. Huang, *J. Power Sources* 278 (2015) 773–781.
- [38] K.V. Emtsev, F. Speck, T. Seyller, L. Ley, J.D. Riley, *Phys. Rev. B* 77 (2008) 155303.
- [39] L. Lai, J.R. Potts, D. Zhan, L. Wang, C.K. Poh, C. Tang, H. Gong, Z. Shen, J. Lin, R.S. Ruoff, *Energy Environ. Sci.* 5 (2012) 7936–7942.
- [40] Y. Su, H. Jiang, Y. Zhu, W. Zou, X. Yang, J. Chen, C. Li, *J. Power Sources* 265 (2014) 246–253.